# On the Mechanism of Activation of the BLUF Domain of AppA†

Wouter Laan,‡,§ Magdalena Gauden,|| Sergey Yeremenko,‡ Rienk van Grondelle,|| John T. M. Kennis,|| and Klaas J. Hellingwerf*,‡,||

*Laboratory for Microbiology, Swammerdam Institute for Life Sciences, BioCentrum, University of Amsterdam, Nieuwe Achtergracht 166, 1018 WV Amsterdam, The Netherlands, and Department of Biophysics, Faculty of Sciences, Vrije Universiteit, De Boelelaan 1081, 1081 HV Amsterdam, The Netherlands*

*Received July 14, 2005; Revised Manuscript Received November 2, 2005*

ABSTRACT: AppA, a transcriptional antirepressor, regulates the steady expression of photosynthesis genes in *Rhodobacter sphaeroides* in response to high-intensity blue light and to redox signals. Its blue-light sensing is mediated by an N-terminal BLUF domain, a member of a novel flavin fold. The photocycle of this domain ($AppA_{5-125}$) includes formation of a slightly red-shifted long-lived signaling state, which is formed directly from the singlet excited state of the flavin on a subnanosecond time scale [Gauden et al. (2005) *Biochemistry 44*, 3653−3662]. The red shift of the absorption spectrum of this signaling state has been attributed to a rearrangement of its hydrogen-bonding interactions with the surrounding apoprotein. In this study we have characterized an AppA mutant with an altered aromatic amino acid: W104F. This mutant exhibits an increased lifetime of the singlet excited state of the flavin chromophore. Most strikingly, however, it shows a 1.5-fold increase in its quantum yield of signaling state formation. In addition, it shows a slightly increased rate of ground-state recovery. On top of this, the presence of imidazole, both in this mutant protein and in the wild-type BLUF domain, significantly accelerates the rate of ground-state recovery, suggesting that this rate is limited by rearrangement of (a) hydrogen bond(s). In total, an ∼700-fold increase in recovery rate has been obtained, which makes the W104F BLUF domain of AppA, for example, suitable for future analyses with step-scan FTIR. The rate of ground-state recovery of the BLUF domain of AppA follows Arrhenius kinetics. This suggests that this domain itself does not undergo large structural changes upon illumination and that the structural transitions in full-length AppA are dominated by interdomain rearrangements.

Photoreceptor proteins contain at least one domain that monitors the spectral and intensity changes of the environmental light conditions and elicit an appropriate response in living organisms. Several photoreceptor families have evolved that absorb light in different regions of the solar spectrum, ranging from UV-A to the far-red. Four different families of blue-light absorbing photoreceptors are known: the xanthopsins, the LOV domains, the cryptochromes, and the recently discovered family of the BLUF[1] domains.

The xanthopsins are mainly found in purple bacteria, and photoactive yellow protein (PYP) from *Halorhodospira halophila* is the best characterized of its members. PYP is the prototypical PAS domain and functions as the photoreceptor for negative phototaxis. PAS domains are a ubiquitous signaling module found in proteins from all kingdoms of life. Detailed knowledge is available for the primary photochemistry and the structural dynamics relevant for PYP function. Its photochemistry is based on cis/trans isomerization of an ethylene bond in its 4-hydroxycinammic acid chromophore (*1*), which ultimately results in partial unfolding of the protein in its signaling state (*2*−*5*).

Interestingly, the other three families all use flavin as their chromophore, but each with very different photochemistry. LOV domains occur in many signal transduction proteins such as the phototropins from plants (*6*), VIVID and WC-1 from the fungus *Neurospora crassa* (*7*, *8*), and YtvA from *Bacillus subtilis* (*9*). They mediate different light responses such as phototropism, chloroplast movement, and control of the circadian rhythm. Signaling state formation in the LOV domains is based on light-induced formation of a metastable covalent adduct between the C4 atom of the flavin and the sulfur atom of a conserved cysteine (*10*). Adduct formation results in conformational changes in the LOV domain (*10*−*13*) which are relayed to the surface where they may lead to disruption of a conserved salt bridge (*14*). Phototropins are serine/threonine kinases and exhibit blue-light-dependent autophosphorylation (*14*). All phototropins contain two LOV domains of which the second (i.e., LOV2) is the most important for the light-regulated kinase activity (*15*). It has been shown for a phototropin LOV2 domain that the light-induced structural changes in the canonical LOV domain lead

† M.G., S.Y., and W.L. were supported by The Netherlands Organization for Scientific Research through the Chemical Sciences Council (NWO-CW). J.T.M.K. was supported by the Life Sciences Council of The Netherlands Organization for Scientific Research (NWO-ALW) via a VIDI fellowship.

* Corresponding author: tel, +31-20-5257055; fax, +31-20-5257056; e-mail, K.Hellingwerf@science.uva.nl.

‡ University of Amsterdam.

§ Current address: School of Chemistry, Purdie Building, The University, St. Andrews, Fife KY16 9ST, Scotland.

|| Vrije Universiteit.

[1] Abbreviations: BLUF, sensor of blue light using FAD/flavin; DAS, decay-associated spectrum; EADS, evolution-associated difference spectrum; FAD, flavin adenine dinucleotide; TLC, thin-layer chromatography.

10.1021/bi051367p CCC: $33.50 
Published on Web 12/01/2005

to unfolding of an α-helix outside the PAS fold, which is involved in regulation of the kinase activity (*16*, *17*).

The cryptochromes are found in lower and higher eukaryotes (including mammals such as *Homo sapiens*), insects (*Drosophila*), plants, algae (*Chlamydomonas*), and one prokaryote (*Synechocystis*), where they are involved in processes such as synchronization of the circadian clock, seed germination, and regulation of pigment synthesis (*18*). They share sequence and structural homology with (bacterial) photolyases (*19*). The photochemistry of cryptochromes is thought to be based on (reversible) electron transfer to the flavin (*20*, *21*), but little is known about the changes in tertiary structure after light activation.

Recently, a novel family of blue-light photoreceptors emerged, the BLUF domains [for sensors of *b*lue *l*ight *u*sing *F*AD (*22*)]. BLUF domains are mainly found in prokaryotes and in one eukaryote (*Euglena gracilis*) and are involved in photophobic responses in *E. gracilis* (*23*), in transcriptional regulation in *Rhodobacter sphaeroides* (*24*), and in phototaxis in *Synechocystis* (*25*).

The photochemistry and structural dynamics underlying signaling state formation in the BLUF domains are at present poorly understood. Five members of this family have been characterized by various spectroscopic techniques: AppA from *Rb. sphaeroides* (e.g., refs *24*, *26*, and *27*), Slr1694 from *Synechocystis* PCC6803 (*28*), YcgF from *Escherichia coli* (*29*), the photoactivated adenylyl cyclase (PAC) from *E. gracilis* (*23*), and Tll0078 from *Thermosynechococcus elongatus* BP-1 (*30*). The most extensively studied BLUF domain containing protein, with respect to both function and photochemistry, is AppA from *Rb. sphaeroides* (*24*, *26*, *27*, *31*−*33*). AppA is a regulatory protein that integrates light and redox signals and functions as a transcriptional antirepressor, controlling the expression of the photosynthesis gene clusters via redox and light-modulated interaction with the repressor PpsR (*24*). When oxygen levels decrease, AppA binds to PpsR, thereby preventing the latter from binding to its DNA targets and allowing transcription of the photosynthesis genes. Blue-light illumination disrupts this interaction, restoring the repressor activity of PpsR. The ground state of AppA shows the two main absorption bands typical for a flavin, located around 370 and 447 nm. Upon illumination, an intermediate is formed which exhibits an ∼10 nm red-shifted absorption spectrum, which decays back to the ground state with a rate of $\sim 1 \times 10^{-3}$ $s^{-1}$ (*24*, *27*). The recovery rate of YcgF is about 2-fold faster (*29*) and that of Slr1694 ∼180-fold (*28*), whereas Tll0078 recovers even ∼700-fold faster (*30*). The signaling state is formed directly from the singlet excited state of the flavin on a subnanosecond to nanosecond time scale with a quantum yield of 0.24 (*32*). It has been suggested that the photochemistry of AppA is based on a change in $\pi-\pi$ stacking between the flavin and an aromatic residue, probably a conserved tyrosine, and a change in hydrogen bonding between the flavin N5 and the conserved tyrosine (*26*). In agreement with this, mutation of this tyrosine has been shown to abolish the primary photochemical reaction (*26*, *27*). In addition, FTIR measurements on Slr1694 and the BLUF domain of AppA indicate that signaling state formation in BLUF domains is accompanied by increased hydrogen bonding between the C(4)═O of the flavin and residues lining the chromophore binding pocket (*28*, *33*). The fact that the recovery reaction of the BLUF domain of AppA and that of Slr1694 are respectively approximately 2 and 4 four times slower in $D_2O$ compared to $H_2O$ (*28*, *33*) indicates that (a) rate-limiting proton-transfer step(s) and/or a change in hydrogen bonding is involved in the recovery process.

Secondary structure predictions suggested that the fold of the BLUF domain is different from the structure of all the known flavin-binding folds. This is confirmed by the recent resolution of the crystal structure of the BLUF domain of AppA from *Rb. sphaeroides* and of the BLUF domain containing protein Tll0078 from *T. elongatus* BP-1 (*34*, *35*). The structure of the BLUF domain adopts an α/β-sandwich fold with a βαββαββ topology. The structure shows a five-stranded β-sheet (four antiparallel strands and one parallel strand), with two helices on top of the sheet. The FAD chromophore binds flat on top of the β-sheet and under the α-helices, with the ribose, phosphate, and adenine moieties extending out into solution. The structure shows no significant structural homology to other flavoproteins, so the BLUF domain does indeed represent a novel flavin-binding fold (*34*, *35*).

The flavin-binding pocket of the BLUF domain of AppA is lined by very hydrophobic side chains (Y21, L34, I37, V38, A43, G52, L54, Y56, F61, L65, V75, M76, I79, V88, I90, W104), with a few polar or charged residues (Q63, Q42, Q80, and H85) in a position to make specific contacts with its nitrogen and oxygen atoms. Of these residues, almost all are conserved within the BLUF domain family, suggesting that they specifically evolved for binding flavin. The side chains of H44, N45, and Q63 jointly make four hydrogen bonds to the flavin. N45 and Q63 are both completely conserved, and H44 is a conserved polar residue in the family of BLUF domains. The amide N of the side chain of Q63 donates hydrogen bonds to both the flavin N5 and the phenolic oxygen of Y21, while the oxygen of the Q63 side chain accepts a hydrogen bond from the highly conserved W104. The highly conserved N45 makes two hydrogen bonds to the flavin pyrimidine ring: Its side-chain nitrogen donates a hydrogen bond to the flavin C(4)═O carbonyl oxygen, while its side-chain oxygen accepts a hydrogen bond from the flavin N3. A similar hydrogen-bonding network is observed in the crystal structure of the ground state of the BLUF protein Tll0078 from *T. elongatus* BP-1. However, in this protein, the conserved Q50 (equivalent to Q63 of AppA) makes two hydrogen bonds to the chromophore: one to the N5 of the flavin and one to the oxygen of the C(4)═O carbonyl group.

This conserved glutamine residue appears to play a central role in the mechanism of photoactivation of BLUF domains, since it is hydrogen bonded to both the flavin and the key tyrosine residue. Indeed, a Q50A mutant of Tll0078 is nonresponsive to light (*35*). Moreover, the key tyrosine is not directly hydrogen bonded to the flavin, nor does it form aromatic stacking interactions with it.

In full-length AppA and in the C-terminally truncated variant $AppA_{1-156}$ (containing residues 1−156), the formation of the signaling state is accompanied by a conformational change that increases the Stokes radius and/or the aggregation state of the protein, as detected by size-exclusion chromatography (*24*, *26*). Also FTIR measurements on the BLUF domain of AppA and Slr1694 revealed light-induced structural changes in the protein, although little structural changes

were detected in the flavin (*28*, *33*). Similarly as in PYP and in LOV domains, it is of interest to know whether the light-induced structural changes in BLUF proteins might reflect functional unfolding.

Here we report additional studies on the mechanism of activation of AppA. We characterize a second site-directed mutant of the BLUF domain with an altered aromatic amino acid (W104F), which, very surprisingly, turns out to display a 1.5-fold increase in quantum yield of signaling state formation as compared to the corresponding wild-type protein. In addition, we show that the extent of unfolding of AppA in its signaling state most probably is very limited in the isolated BLUF domain (residues 5−125). This conclusion is based on the linear Arrhenius kinetics of its ground-state recovery rate. This recovery rate can be accelerated up to 700-fold, which makes this BLUF domain suitable for studies that require high repetition rates of photoactivation, like step-scan FTIR. Kinetic isotope effects lead to the conclusion that important transitions that are not reflected in altered UV−vis flavin spectra are involved in the photocycle of this BLUF domain.

## MATERIALS AND METHODS

*Strains and Growth Conditions.* Cloning was performed using *E. coli* XL1-Blue grown in LB medium according to established protocols. Protein overproduction was performed in *E. coli* M15 (pREP4) grown in production broth (PB: 20 g $L^{-1}$ tryptone, 10 g $L^{-1}$ yeast extract, 5 g $L^{-1}$ dextrose, 5 g $L^{-1}$ NaCl, and 8.7 g $L^{-1}$ $K_2HPO_4$, pH 7.0). Ampicillin and kanamycin were used at 100 and 50 $\mu$g $mL^{-1}$, respectively.

*Site-Directed Mutagenesis.* The BLUF domain with the W104F mutation was constructed with the QuickChange site-directed mutagenesis kit (Stratagene, La Jolla, CA). pQEAppA$_{5-125}$ (*27*) was used as the template for the PCR reaction using the following primers: AppA W104F F, 5′-GCTTTGCGGGAT**TT**CACATGCAGCTCTCCTGC-3, and AppA W104F R, 5′-GCAGGAGAGCTGCATGTG**AA**ATC-CCGCAAAGC-3′. Mutated bases are indicated in bold. The constructs were verified by sequencing (BaseClear, Leiden, The Netherlands).

*Protein Production and Purification.* Wild-type AppA$_{5-125}$ and the AppA$_{5-125}$ W104F mutant were both expressed and purified essentially as described previously (*36*). Before proceeding with the nickel purification, the cell-free extracts were incubated for 1 h on ice with a large molar excess of FAD. Purified proteins were dialyzed to 10 mM Tris-HCl, pH 8.0, and stored at −20 °C. Purity of the samples was checked by SDS−PAGE using the PHAST System (Amersham Biosciences) and UV−vis spectroscopy. The flavin composition of each variant was determined by thin-layer chromatography (TLC) as described (*36*). For isotopic replacement, the protein was concentrated and subsequently diluted with buffered $D_2O$ at least three times.

*Transient UV−Vis Absorption Spectroscopy.* Steady-state UV−vis absorption spectra and receptor state recovery kinetics were recorded using a Hewlett-Packard 8453 spectrophotometer (Portland, OR). Measurements of the rate of receptor state recovery were performed using a "Kraayenhof vessel" (*37*) placed in the sample compartment of the spectrophotometer. One port of the vessel was used to convert AppA (WT or W104F in 10 mM Tris-HCl, pH 8.0, with or without different concentrations of salt or imidazole as indicated in the Results section) to the signaling state by illumination with actinic light from a Schott KL1500 light source (containing a 150 W halogen lamp). Two ports were used for the measuring beam, and the fourth port was used to monitor the pH by using a Mettler Toledo (micro) combination pH electrode (InLab423) connected to a Dulas Engineering amplifier. The data were fitted with a monoexponential decay function using Origin software.

*Ultrafast Time-Resolved Spectroscopy.* Time-resolved fluorescence experiments were performed with a synchroscan streak camera setup described earlier (*38*). The time-resolved fluorescence kinetics were recorded upon excitation at 400 nm at a power of 500 $\mu$W. Pulses of 100 fs duration were generated with 50 kHz repetition rate using an amplified titanium:sapphire laser system (Vitesse-DUO-Rega, Coherent Inc., Mountain View, CA). Fluorescence was collected with a right-angle detection geometry using achromatic lenses and detected through a sheet polarizer set at the magic angle (54.7°) with a Hamamatsu C5680 synchroscan camera and a Chromex 250IS spectrograph. The streak images were recorded with a cooled (−55 °C) Hamamatsu C4880 CCD camera. Streak camera images were obtained on time bases of 200 ps and of 2 ns.

Femtosecond transient absorption spectroscopy was carried out with a 1 kHz Ti:sapphire-based regenerative amplification system described previously (*39*); 400 nm light was obtained by frequency doubling the output of the Ti:sapphire laser, attenuated to 1 $\mu$J, and used as a pump. A white light continuum, generated by focusing the rest of the amplified 800 nm light on a 1 mm $CaF_2$ crystal, was used as a probe. The probe pulse was focused and overlapped with the excitation beam at the sample position. After passing through the sample, the probe beam was dispersed by a polychromator and projected on a diode array detector. Femtosecond time delays between the pump and probe were controlled by a delay line covering delays up to 4.5 ns. The relative polarization plane of the pump and probe beams was set to the magic angle (54.7°).

The samples were loaded in a flow system with a volume of 10 mL, including a flow cuvette with a path length of 1 mm, and passed by a peristaltic pump. For the time-resolved fluorescence experiment, the absorbance of the sample was adjusted to 0.07 $mm^{-1}$ at 446 nm, whereas for the femtosecond time-resolved absorption experiment, the absorbance of the sample was adjusted to 0.3 $mm^{-1}$. The absorption spectrum of the sample was checked during the measurements to verify that the sample remained in the "dark" state.

*Data Analysis.* The time-resolved fluorescence data were globally analyzed in terms of a sum of exponentials to obtain decay-associated spectra (DAS). The femtosecond transient absorption data were globally analyzed using a kinetic model consisting of sequentially interconverting evolution-associated difference spectra (EADS), i.e., 1 → 2 → 3 → ... in which the arrows indicate successive monoexponential decays of increasing time constant, which can be regarded as the lifetime of each EADS. The first EADS corresponds to the time zero difference spectrum. This procedure enables us to visualize clearly the evolution of the (excited) states of the system. In general, the EADS may well reflect mixtures of molecular states. The instrument response

function was fit to a Gaussian of 120 fs full width at half-maximum for the ultrafast transient absorption experiments and 3 and 13 ps for the time-resolved fluorescence measurements on the 200 ps and 2 ns time base, respectively. The global analysis procedures described in this paper have been extensively reviewed in ref *40*.

*Calculation of Thermodynamic Parameters.* Thermodynamic parameters were calculated using eq 1, in which $k_{gr}$ is the rate of ground-state recovery and $h$, $k_b$, and $R$ are the Planck, Boltzmann, and universal gas constant, respectively.

$$\ln\frac{k_{gr}h}{k_bT} = \frac{\Delta S_i^{\ddagger}(T_0)}{R} - \frac{\Delta H_i^{\ddagger}(T_0)}{RT} - \frac{\Delta C_{pi}^{\ddagger}}{R}\left(1 - \frac{T_0}{T} + \ln\frac{T_0}{T}\right) \quad (1)$$

*Quantum Yield of Signaling State Formation of AppA$_{5-125}$ W104F.* The quantum yield of signaling state formation of the W104F mutant was determined using a relative actinometric method with ruthenium(II) trisbipyridine [Ru(bpy)$_3^{2+}$] as a reference, as described for the wild-type BLUF domain of AppA (*32*), assuming the same extinction coefficient at 447 nm as for the wild-type protein [8500 $M^{-1}$ $cm^{-1}$ (*26*)]. The quantum yield of signaling state formation in AppA was determined using the expression:

$$\Phi_{AppA} = \Phi_{ref}\frac{\Delta OD_{AppA}^{(495)}\Delta\epsilon_{ref}^{(450)}}{\Delta OD_{ref}^{(450)}\Delta\epsilon_{AppA}^{(495)}} \quad (2)$$

where $\Phi_{ref}$ is the quantum yield of the photoreaction of Ru(bpy)$_3^{2+}$, $\Delta\epsilon_{ref}^{(450)}$ ($M^{-1}$ $cm^{-1}$) is the change in the absorption coefficient of Ru(bpy)$_3^{2+}$ at 450 nm, $\Delta\epsilon_{AppA}^{(495)}$ ($M^{-1}$ $cm^{-1}$) is the change in the absorption coefficient of AppA at 495 nm, and $\Delta$OD is the optical density change.

## RESULTS

*Characterization of AppA W104F.* Ultrafast fluorescence and femtosecond to nanosecond transient absorption spectroscopy measurements on AppA have revealed that the signaling state of AppA is formed directly from the singlet excited state of the flavin on a subnanosecond to nanosecond time scale with a quantum yield of 0.24 (*32*). Given that the natural lifetime of a flavin cofactor amounts to several nanoseconds, these results indicated that an additional excited-state deactivation mechanism had to be in effect in AppA. Tryptophan residues are well-known as electron donors, and a tryptophan, at position 104 in the BLUF domain of AppA, is highly conserved in all known BLUF sequences. To explore the potential role of this residue in the photochemistry of AppA, we changed this tryptophan to a phenylalanine and produced and purified this W104F protein. The protein was produced with yields comparable to those of the wild-type protein and could be fully reconstituted with FAD exclusively (data not shown). The W104F variant was photoactive, and the UV−vis absorption spectra of its ground and signaling state and the light minus dark difference spectrum are similar to those of the wild type, although the spectrum of the signaling state is a little less far-red shifted, exhibiting absorption maxima at 457 and 380 nm [460 and 381 nm in wild type (Figure 1)]. As in the wild type, the signaling state of the mutant protein returns back to the ground state monoexponentially, however, with

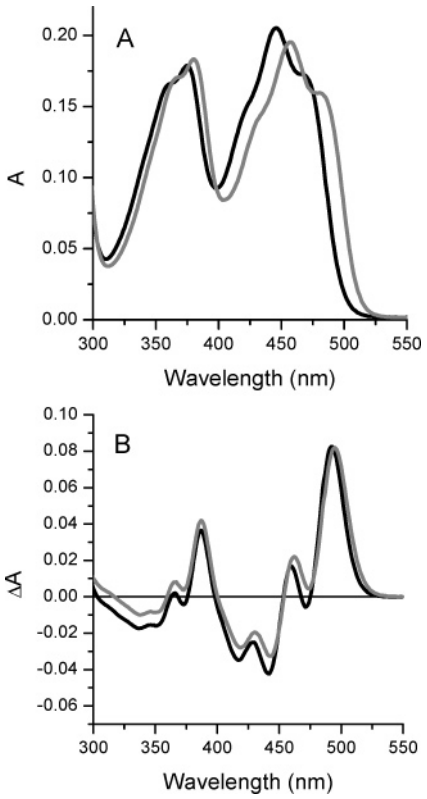


FIGURE 1: UV−vis absorption characteristics of the W104F mutant. (A) Absorption spectra of the W104F variant (in 10 mM Tris-HCl, pH 8.0 at 25 °C) in the dark (black line) and after illumination (gray line). (B) Light minus dark difference spectra of the W104F mutant (black line) and wild-type AppA$_{5-125}$ (gray line).

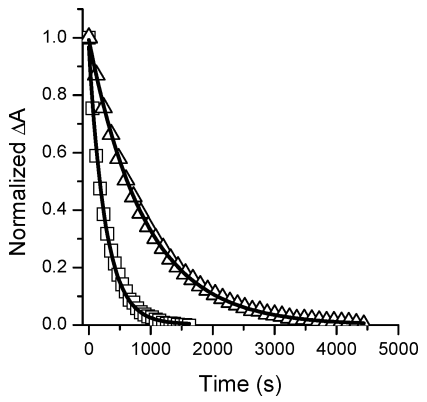


FIGURE 2: Recovery kinetics of the W104F mutant. AppA$_{5-125}$ W104F (squares) and wild-type AppA$_{5-125}$ (triangles, both in 10 mM Tris-HCl, pH 8.0 at 25 °C) were converted to the signaling state by illumination with white light and allowed to revert back to the ground state in the dark. Plotted are the absorption changes at 495 nm. The solid lines represent fits through the data using a monoexponential function. The corresponding recovery rates are given in Table 2.

a 2.7-fold increased recovery rate (Figure 2). The ratio of the absorption at 270 nm over the absorption of the flavin peak at 447 nm is ~90% of that of the wild type (data not shown), which can be accounted for by a decrease in the intensity of the 270 nm peak by replacement of a tryptophan ($\epsilon_{270}$ = 5200 $M^{-1}$ $cm^{-1}$) by a phenylalanine ($\epsilon_{259}$ = 200 $M^{-1}$ $cm^{-1}$). This suggests that the extinction coefficient of the flavin is unaffected by the W104F mutation.

We also determined the quantum yield of signaling state formation using the relative actinometric method with Ru-

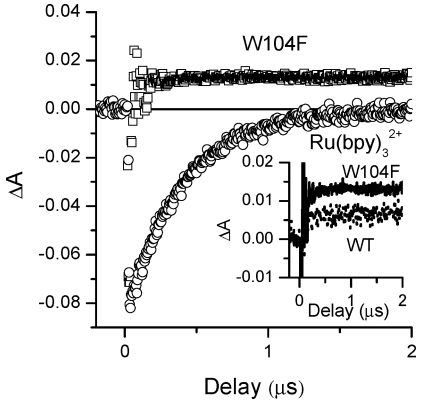


FIGURE 3: Quantum yield determination of signaling state formation of AppA W104F. Transient absorption kinetics of solutions of Ru(bpy)$_3^{2+}$ (circles) and AppA W104F (squares) measured at 450 and 495 nm, respectively, after excitation by a laser pulse at 450 nm. The inset shows the absorption changes after excitation at 450 nm for both the wild-type and the mutant protein. The quantum yield was calculated using eq 2. Note that the signal at 495 nm shows some variation as a result from interference with the Q-switch from the Nd:YAG laser.

(bpy)$_3^{2+}$ as a reference, which we have previously used to determine the quantum yield of wild-type AppA. The photoreactions were monitored by the detection of transient absorption changes at 450 and 495 nm for the reference and AppA, respectively, after their excitation at 450 nm. To determine the quantum yield, absorbance changes of the samples at the time of appearance of the maximal concentration of the photoproduct state were assessed (Figure 3). Very surprisingly, the W104F mutant protein displayed larger absorption changes at 495 nm than the wild-type protein (see Figure 3 inset), suggesting a higher quantum yield for the former. Indeed, using actual experimental parameters, the quantum yield of the phototransformation is determined as follows: $\Phi_{\text{AppA W104F}} = (0.013 \times 7900)/(0.08 \times 3500) = 0.37 \pm 0.07$, which is 1.5-fold higher than the quantum yield determined for the wild-type protein.

*Time-Resolved Fluorescence Spectroscopy.* To try to determine the basis for the observed increased quantum yield of the W104F mutant, we have performed synchroscan streak camera fluorescence experiments to examine its excited-state dynamics and compared these with results obtained for the wild-type protein in a previous study (*32*). The selected excitation wavelength was 400 nm, which implies that a mixture of $S_1$ and $S_2$ singlet excited states of FAD was generated. The fluorescence was monitored in a spectral window from 460 to 650 nm. A kinetic trace (gray line) measured at the maximum of the fluorescence emission band (505 nm) is depicted in Figure 4B, together with a trace measured on the WT protein for comparison (black line). As becomes evident from Figure 4B, the W104F mutant has a longer excited-state lifetime than wild-type AppA. The application of a global analysis procedure yielded three decay components, with lifetimes of 47 ps, 555 ps, and 2.5 ns. The solid lines in Figure 4B show the fitted curves. The decay-associated spectrum (DAS) of each component (Figure 4A) has a maximum around 505 nm and a shoulder around 530 nm. The DAS of the first component is blue shifted compared to the other two, but this DAS may be affected by a scattering contribution from the 400 nm excitation pulse. The 555 ps component is dominant with a decay amplitude of 0.63, with

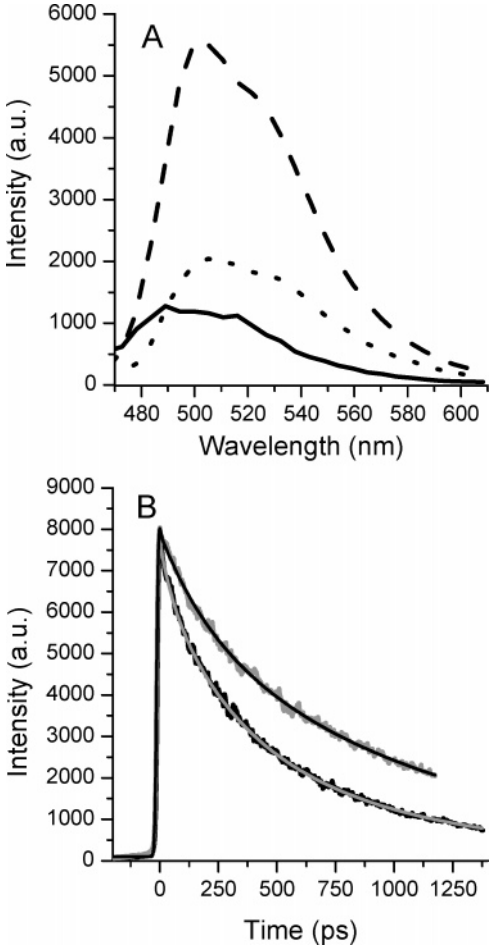


FIGURE 4: Time-resolved fluorescence of AppA W104F. (A) Decay-associated spectra (DAS) with time constants of 47 ps (black line), 555 ps (dashed line) and 2.5 ns (dotted line) that follow from a global analysis of the streak camera images obtained from AppA W104F upon 400 nm excitation. (B) Time-resolved fluorescence trace recorded at 505 nm of wild-type AppA (bottom black line) and AppA W104F (top gray line) and results of the global analysis fitting procedure (gray and black line for wild-type and W104F, respectively).

smaller contributions by the 47 ps component (amplitude 0.14) and the 2.5 ns component (0.23). These data are significantly different from those obtained on the wild-type protein. In the wild type, four components were observed: 25 ps (amplitude 0.10), 150 ps (amplitude 0.32), 670 ps (amplitude 0.56), and 3.8 ns (amplitude 0.02). The kinetics of the fastest component in AppA W104F is similar to that of the fastest component in the wild-type protein, also with respect to amplitude. The dominant 555 ps may be compared with the 670 ps component in the wild type. The slowest component of the mutant has a shorter lifetime than the slowest component in the wild type, but a 10-fold increased contribution, whereas the 150 ps component in the wild type has no counterpart in the mutant. This results in an overall increase in the lifetime of the singlet excited state of the chromophore in the mutant, as compared to the wild-type protein, which may be related to the increased quantum yield of signaling state formation, as will be discussed below.

*$D_2O$ and Imidazole Affect the Ground-State Recovery Rate.* Figure 5A shows the decay kinetics of the signaling state of $AppA_{5-125}$ in $H_2O$ and $D_2O$. The deuterated sample exhibits a 4.7-fold slower recovery rate. This deceleration is com-

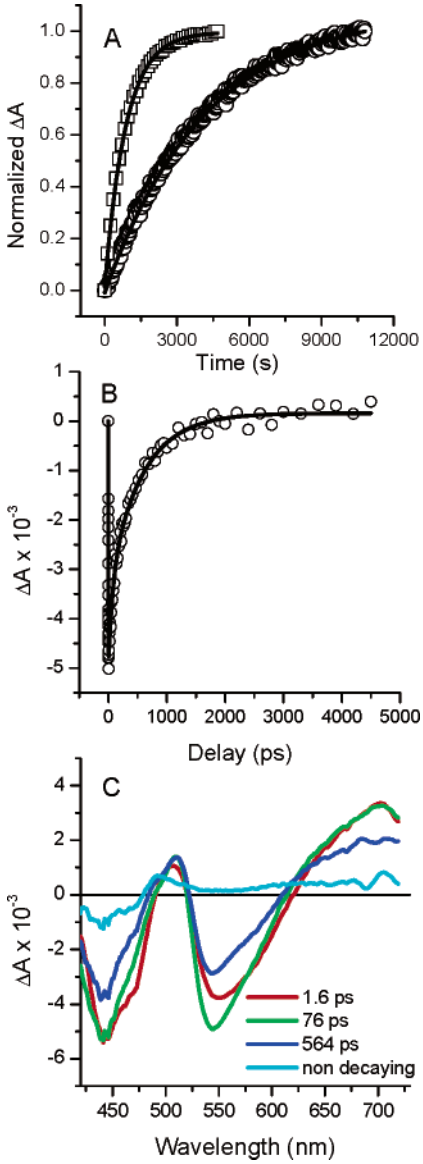


FIGURE 5: Photocycle kinetics of $AppA_{5-125}$ in $D_2O$. (A) $AppA_{5-125}$ in $H_2O$ (squares) and $AppA_{5-125}$ in $D_2O$ (circles, both in 10 mM $K/PO_4$, pH 8.0 at room temperature) were converted to the signaling state by illumination with white light and allowed to revert back to the ground state in the dark. Plotted are the absorption changes at 447 nm. The solid lines represent fits through the data using a monoexponential function. (B) Ultrafast kinetic trace at 546 nm of $AppA_{5-125}$ in $D_2O$ upon excitation at 400 nm (circles), along with the result of the global analysis of these data (solid line). (C) Evolution-associated difference spectra (EADS) and their corresponding lifetimes resulting from global analysis of ultrafast transient absorption experiments on $AppA_{5-125}$ in $D_2O$ upon excitation at 400 nm.

parable to what has been observed for Slr1694, although in absolute terms the recovery rates in Slr1694 are ~200-fold higher than in AppA. It should be noted that this deceleration of the rate of recovery by $D_2O$ is considerably more pronounced than the ~2-fold reduction reported previously for the BLUF domain of AppA (*28*, *33*).

To assess whether deuteration of the BLUF domain affects the kinetics of signaling state formation, we performed femtosecond time-resolved absorption spectroscopy on this domain in $D_2O$. The EADS that result from the sequential analysis are presented in Figure 5C, while the solid line in Figure 5B represents the fit to a kinetic trace taken at 546 nm, at the maximum of the stimulated emission band of the FAD chromophore. Four kinetic components are required for a satisfactory fit of the time-resolved data, with time constants of 1.6, 76, and 564 ps and a nondecaying component. The first EADS (red line) is created upon photon absorption and shows ground-state bleaching features near 450 nm, a small excited-state absorption near 520 nm, a stimulated emission band near 550 nm, and excited-state absorption at wavelengths longer than ~620 nm, indicating the presence of the singlet excited state of the flavin chromophore (*32*, *41*, *42*). This EADS lives for 1.6 ps, and it evolved into the second EADS which has a lifetime of 76 ps (green line). This evolution involves a small blue shift and increase of the stimulated emission band near 550 nm and is assigned to a vibrational cooling process of the excited FAD (*32*). Thus, the second EADS corresponds to the relaxed singlet excited state of FAD. Next, the second EADS evolves into the third EADS (blue line) in 76 ps. This EADS has decreased amplitude of ground-state bleach, stimulated emission and excited-state absorption bands, indicating decay of excited FAD. As observed in hydrated AppA, a small shoulder is visible near 495 nm on top of the excited FAD excited-state absorption, which indicates that during the 76 ps evolution a fraction of the signaling state is formed. The third EADS evolves in the nondecaying EADS (cyan line) in 564 ps. In the final EADS, the singlet excited states of FAD have all but disappeared, and an absorption band at 495 nm has formed, whereas a small ground-state bleach near 450 nm and induced absorption near 650 nm have remained. As observed previously in hydrated AppA, the absorption band at 495 nm corresponds to formation of the AppA signaling state, whereas the absorption near 650 nm may be assigned to formation of a small number of triplet states of FAD (*32*).

Compared to the results obtained on the BLUF domain in $H_2O$ in our previous study (*32*), both the fastest and slowest component (250 fs and 2.7 ns) are not resolved in the analysis of the deuterated sample. The components that are resolved are spectrally and kinetically comparable to those observed in $H_2O$. The 1.6 ps component in the deuterated sample may be compared to the 1.2 ps component in the hydrated sample, where it has been attributed to vibrational cooling. The 76 and 564 ps component may be compared to the 90 and 590 ps component, respectively, observed in the hydrated sample, which represent the decay of the singlet excited state of the flavin to the electronic ground state of the signaling state and to decay to the ground state of dark AppA (*32*). The 250 fs component, observed in hydrated AppA, was not resolved here because of the presence of a pronounced cross-phase modulation artifact in the data, which obscured the dynamics around time zero. Also, in hydrated AppA we observed a very small spectral evolution on the nanosecond time scale. Here, we could not resolve such a component because of a less favorable signal to noise ratio.

During purification of the BLUF domain of AppA it was observed that the recovery rate of the protein directly after elution from the nickel affinity column, thus in the presence of 0.5 M NaCl plus 0.5 M imidazole, was significantly higher than after dialysis against buffer without salt and imidazole. Analysis of the recovery rate in the presence of either NaCl or imidazole revealed that the observed effect is mainly due to imidazole (Table 2). The recovery rate increased 1.5-fold

Table 1: Thermodynamic Parameters of the Ground-State Recovery of AppA[a]

| $\Delta S^{\ddagger}$ [J/(mol·K)] | $\Delta H^{\ddagger}$ (kJ/mol) | $\Delta G^{\ddagger}$ (kJ/mol) | $\Delta C_p^{\ddagger}$ [J/(mol·K)] |
|---|---|---|---|
| 71 ± 11 | 82 ± 3 | 61 ± 9 | 570 ± 490 |

[a] The values of the thermodynamic activation parameters associated with the recovery of $AppA_{5-125}$ were calculated from the fit of the data from Figure 1. Values at 298 K are shown, followed by the standard deviation in the thermodynamic parameter, according to the least-squares fit of the data to eq 1.

Table 2: NaCl and Imidazole Increase the Recovery Rate of AppA[a]

| protein | pH | NaCl (M) | imidazole (M) | rate ($\times 10^{-3}$ $s^{-1}$) |
|---|---|---|---|---|
| wild type | 8.0 | 0 | 0 | 1.30 ± 0.10 |
| wild type | 8.0 | 0.5 | 0 | 1.62 ± 0.03 |
| wild type | 8.0 | 1.0 | 0 | 2.04 ± 0.20 |
| wild type | 8.0 | 0 | 0.5 | 19.50 ± 1.50 |
| wild type | 8.0 | 0 | 1.0 | 34.70 ± 0.20 |
| wild type | 8.0 | 0 | 1.5 | 68.30 ± 1.68 |
| wild type | 8.0 | 0 | 2.0 | 104.63 ± 1.72 |
| wild type | 7.0 | 0 | 0 | 1.50 ± 0.08 |
| wild type | 7.0 | 0 | 1 | 18.68 ± 0.30 |
| W104F | 8.0 | 0 | 0 | 3.55 ± 0.04 |
| W104F | 8.0 | 0 | 0.5 | 82.60 ± 1.00 |
| W104F | 8.0 | 0 | 1.0 | 201.12 ± 9.40 |
| W104F | 8.0 | 0 | 1.5 | 479.40 ± 17.0 |
| W104F | 8.0 | 0 | 2.0 | 730.56 ± 33.7 |

[a] The recovery of wild-type $AppA_{5-125}$ and the W104F mutant protein was measured at 25 °C in 10 mM Tris-HCl, pH 7.0 or 8.0, in the absence or presence of NaCl and imidazole. The absorption changes at 495 nm were fitted with a monoexponential function. The values shown are the mean of at least two experiments and the standard deviation.

in the presence of 1 M NaCl, whereas an equal concentration of imidazole increased the recovery rate 27-fold (Figure 6). Concentrations of imidazole up to 2 M, at which the recovery is ~80 times faster, did not significantly affect the UV−vis spectra of the ground and signaling state but higher concentrations resulted in release of the flavin from the apoprotein, as indicated by a simultaneous loss of fine structure and red shift of the ground-state UV−vis spectrum. The recovery rate shows a linear dependence on the imidazole concentration, indicating a first-order effect. The recovery was monoexponential, indicating that the imidazole does not induce formation of additional intermediates (Figure 6). Imidazole has a p*K* of 6.95, and the fact that the increase in recovery rate in the presence of 1 M imidazole is about 2-fold smaller at pH 7 (53% neutral imidazole) compared to pH 8 (92% neutral imidazole) suggests that it is the neutral form of imidazole that affects the recovery kinetics. The recovery kinetics of the protein before the addition of imidazole and after removal of the imidazole by dialysis were identical. This shows that the effect exerted by the imidazole is reversible. As observed for the wild-type protein, imidazole also significantly increased the ground-state recovery rate of AppA W104F, ultimately resulting in an ~700-fold acceleration at 2 M imidazole compared to wild-type protein without imidazole (Table 2). Significantly, the recovery rate in the W104F derivative is always faster (between 2.7- and 7-fold under the conditions tested) than the corresponding rate in the wild-type BLUF domain of AppA.

*Thermodynamics of the Recovery.* It has been suggested, based on size-exclusion chromatography of full-length AppA and the C-terminally truncated variant $AppA_{1-156}$, that light

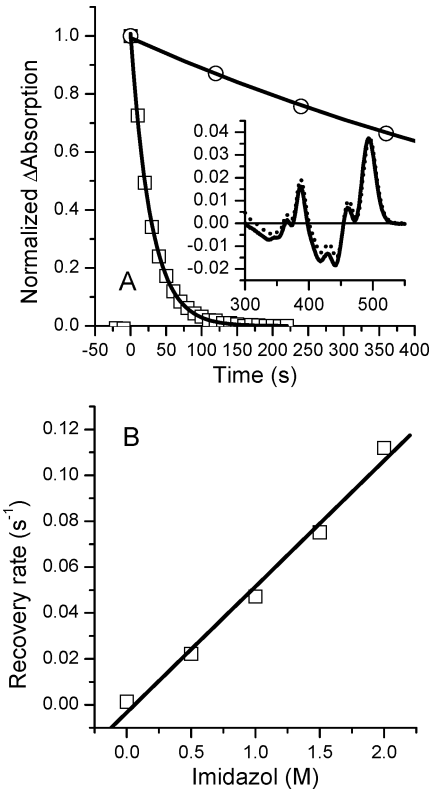


FIGURE 6: Effect of imidazole on the recovery rate of AppA. (A) $AppA_{5-125}$ (in 10 mM Tris-HCl, pH 8.0 at 25 °C) with (squares) or without 1 M imidazole (circles) was converted to the signaling state by illumination with white light and allowed to revert back to the ground state in the dark. The solid lines represent fits through the data points using a monoexponential (decay) function. The insert shows the UV−vis light minus dark difference spectra of AppA with (solid line) and without 1 M imidazole (dotted line). (B) Plot of the ground-state recovery rate of $AppA_{5-125}$ as a function of the imidazole concentration. The data points are taken from Table 2. The error in each point is smaller than 3%. The line represents a linear fit through the data points.

induces a conformational change in the protein that increases the Stokes radius. Similar experiments also show that the full-length protein is a monomer, whereas $AppA_{1-156}$ forms dimers (*24*, 26). Analysis of $AppA_{5-125}$ by size-exclusion chromatography (using a preilluminated sample and illuminating the column during chromatography with a 150 W lamp) has revealed no significant difference in elution profile between the ground and signaling state of AppA. Both states elute at a volume corresponding to an ~40 kDa protein (data not shown). Since the mass of the protein is 15.5 kDa, this indicates that also this variant forms dimers. The apparent molecular mass (40 kDa) is higher than the mass of a dimer calculated from the amino acid sequence (31 kDa), suggesting that $AppA_{5-125}$ forms dimers with a molecular shape that deviates from a sphere (*43*). A change in the tertiary structure of a protein, like partial unfolding, may result in a change in heat capacity, as has been shown for PYP (*4*, *44*, *45*). The change in heat capacity associated with the transition from the signaling to the ground state of a photoreceptor protein can be calculated from the degree of curvature of a plot of the natural logarithm of the recovery rate against reciprocal temperature, i.e., an Arrhenius plot. For the BLUF domain of AppA, a nearly linear plot is obtained (Figure 7). From this plot, a change in heat capacity associated with the transition from the signaling to the ground state of 570

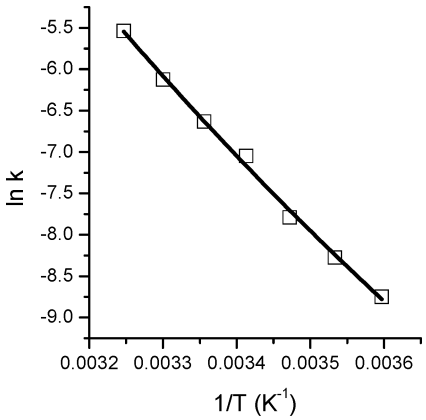


FIGURE 7: Thermodynamic analysis of the rate of ground-state recovery of $AppA_{5-125}$. The natural logarithm of the rate constant *k* is plotted as a function of reciprocal temperature. The points shown are the mean of at least two experiments; the error in each point is less than 5%. The solid line represents the fit to the data using eq 1.

J/mol/K can be calculated, albeit with a large uncertainty (Table 1). This value is about 5-fold smaller, and of opposite sign, than the value reported for PYP [−2.5 kJ/(mol·K) (*4*, *45*)].

## DISCUSSION

The fact that the recovery rate of the W104F mutant is slightly increased compared to the wild type might indicate that the signaling state of this variant is less stable than the light-induced state of the wild type. The reduced temperature stability of the mutant is in agreement with this (data not shown). The increased quantum yield of signaling state formation might be related to the longer living singlet excited state of the flavin, as shown by time-resolved fluorescence measurements. As we noted earlier, to explain the fluorescence lifetime in wild-type AppA, a singlet excited-state deactivation mechanism must be active that competes with signaling state formation (*32*). It has been shown in flavoenzymes already that efficient electron and proton transfer may occur from aromatic residues to the flavin, after which the radical pair rapidly recombines on the picosecond time scale to the ground state (*46*, *47*). We propose that, in wild-type AppA, the FAD singlet excited state is partially deactivated via a hydrogen transfer, an electron transfer, or a coupled electron−proton transfer from Trp104 to FAD (e.g., possibly in competition with electron transfer from Y21) and subsequent rapid recombination to the ground state. If this recombination is faster than the initial electron/hydrogen transfer, the semiquinone will not transiently accumulate in an appreciable concentration and, thus, will not be detected. In the W104F mutant, the contribution of this deactivation pathway would be significantly reduced due to the lower electron/proton-transfer capacities of the phenylalanine, resulting in a longer excited-state lifetime and increased quantum yield of signaling state formation, consistent with our present results.

The rate of electron/hydrogen transfer is dependent on the donor/acceptor distance. In flavoproteins where ultrafast electron/hydrogen transfer from a Trp residue to the flavin is observed (e.g., in flavodoxin, photolyase), the edge to edge distance between the Trp and the flavin is about 3−4 Å (*46*−*48*). In agreement with this, the distance between the side chain of W104 and the flavin C(4)═O oxygen is about 3 Å in the crystal structure of the BLUF domain of AppA (*34*). It is interesting to note that ultrafast transient absorption measurements on Y21 mutants revealed spectral features that were consistent with the transient presence of a neutral flavin semiquinone, a species which is not observed in the wild type (Gauden et al., unpublished experiments). Since the samples did not contain any reducing agent, the hydrogen atom taken up by the flavin must originate from the protein environment, and in light of the present results, W104 would be a very likely donor.

Trp104 is almost completely conserved in all of the BLUF sequences known to date. The exceptions are the second BLUF domain of the PACα subunit from *E. gracilis* (which contains a leucine at this position), the two BLUF domains from *Klebsiella pneumoniae* (threonine and valine), and YcgF from *E. coli* (alanine). It would be of interest to determine the quantum yield of signaling state formation of these BLUF domains and assess whether the introduction of a Trp at this position would also decrease the quantum yield in these BLUF domains.

The reduction of the ground-state recovery rate of AppA in $D_2O$ is comparable to the reduction observed in Slr1694 but is significantly larger than the 2-fold reduction reported by ref *33* for the BLUF domain of AppA. The reason for this difference is at present unclear. The effect of deuteration indicates that ground-state recovery involves a rate-limiting rearrangement of hydrogen bonds and/or a proton-transfer step. Formation of the signaling state has been proposed to involve a change in hydrogen bonding between the conserved tyrosine and the flavin (*26*). However, the crystal structure of the BLUF domain reveals that the conserved tyrosine is indirectly hydrogen bonded to the flavin via a conserved glutamine. The role of the tyrosine appears to be to keep the glutamine positioned close to the flavin. Presumably, light activation of the BLUF domain leads to a reorientation of the glutamine side chain with respect to the flavin, leading to increased strength of hydrogen bonding at the C(4)═O (*34*). Surprisingly, deuteration does not have a significant effect on the kinetics of formation of the red-shifted state. Although we can at present not exclude that a kinetic isotope effect underlies the slightly slower vibrational cooling after excitation of the flavin in the BLUF domain of AppA in $D_2O$ (1.6 vs 1.2 ps in $H_2O$), the kinetics of the formation of the signaling state are, within experimental error, identical. This suggests that the recovery of the ground state is not simply a reversal of the light-induced events leading to the signaling state but involves a different mechanism.

In contrast to deuteration, the presence of imidazole significantly accelerates ground-state recovery. The structure of imidazole is analogous to the side chain of histidine, which is capable of accepting and donating hydrogen bonds. Imidazole might increase the rate of ground-state recovery by catalyzing the relaxation of the light-induced changes in the hydrogen-bonding network of AppA. However, the fact that the UV−vis spectra of both the ground and the signaling state are virtually unaffected by the presence of imidazole suggests that imidazole affects the protein outside the chromophore binding pocket.

By combining the effects of the W104F mutation and those of addition of imidazole, ground-state recovery rates are obtained which are compatible with step-scan FTIR. This

will be very useful to gain more insight into the detailed structural dynamics underlying the BLUF photocycle.

We conclude that the BLUF domain of AppA displays relatively restricted structural changes upon illumination, although a recent FTIR study did reveal such changes (*33*). The linear Arrhenius behavior of the ground-state recovery of the BLUF domain of AppA indicates that there is no significant change in heat capacity between the ground and signaling state. Although this does not exclude the possibility that illumination elicits a large structural change without exposure or shielding of a hydrophobic surface, both our results of size-exclusion chromatography and the fact that we observe very little changes in the structure of AppA upon illumination in HSQC NMR spectra (Hsu et al., unpublished experiments) argue against such a large conformational transition and rather suggest that these changes are minor. The positive value for the change in heat capacity suggests that, in contrast to what is observed in PYP, signaling state formation in $AppA_{5-125}$ results in burial of hydrophobic contact surface. The fact that an apparent increase in size upon illumination is observed with the BLUF domain in the context of longer fragments of AppA suggests that the minor structural changes in the BLUF domain upon formation of the signaling state propagate to residues outside the domain and lead to larger structural changes in elements outside the BLUF domain.

A fragment of AppA lacking the entire BLUF domain is still functional with respect to redox signaling, implying that the C-terminal part of AppA interacts with PpsR (*49*, *50*). Upon illumination of the full-length protein this interaction is disrupted, suggesting that the light-induced structural changes in the BLUF domain are propagated to the C-terminal domain of AppA. A similar mechanism is observed in PYP and LOV domains, where light-induced structural changes in the PAS core of the protein lead to partial unfolding of helical segments outside the PAS domain. It would therefore be of interest to determine whether longer fragments of AppA show nonlinear Arrhenius behavior of their ground-state recovery kinetics.

The fact that $AppA_{5-125}$ and $AppA_{1-156}$ both form dimers, whereas the full-length protein is a monomer in solution, suggests that truncation of AppA exposes a hydrophobic region in the protein which is stabilized by protein−protein interactions. In the full-length protein, this putative interaction surface might relay the structural changes in the BLUF domain to the C-terminal domain.

## REFERENCES


1. Kort, R., Vonk, H., Xu, X., Hoff, W. D., Crielaard W., and Hellingwerf, K. J. (1996) Evidence for trans-cis isomerization of the *p*-coumaric acid chromophore as the photochemical basis of the photocycle of photoactive yellow protein, *FEBS Lett. 38*, 73−78.
2. Chen, E., Gensch, T., Gross, A. B., Hendriks, J., Hellingwerf, K. J., and Kliger, D. S. (2003) Dynamics of protein and chromophore structural changes in the photocycle of photoactive yellow protein monitored by time-resolved optical rotatory dispersion, *Biochemistry 42*, 2062−2071.
3. Craven, C. J., Derix, N. M., Hendriks, J., Boelens, R., Hellingwerf, K. J., and Kaptein, R. (2000) Probing the nature of the blue-shifted intermediate of photoactive yellow protein in solution by NMR: hydrogen−deuterium exchange data and pH studies, *Biochemistry 39*, 14392−14399.
4. Van Brederode, M. E., Hoff, W. D., Van Stokkum, I. H., Groot, M. L., and Hellingwerf, K. J. (1996) Protein folding thermodynamics applied to the photocycle of the photoactive yellow protein, *Biophys. J. 71*, 365−380.
5. Rubinstenn, G., Vuister, G. W., Mulder, F. A., Dux, P. E., Boelens, R., Hellingwerf, K. J., and Kaptein, R. (1998) Structural and dynamic changes of photoactive yellow protein during its photocycle in solution, *Nat. Struct. Biol. 5*, 568−570.
6. Huala, E., Oeller, P. W., Liscum, E., Han, I. S., Larsen, E., and Briggs, W. R. (1997) Arabidopsis NPH1: a protein kinase with a putative redox-sensing domain, *Science 278*, 2120−2123.
7. Ballario, P., Talora, C., Galli, D., Linden, H., and Macino, G. (1998) Roles in dimerization and blue light photoresponse of the PAS and LOV domains of *Neurospora crassa* white collar proteins, *Mol. Microbiol. 29*, 719−729.
8. Heintzen, C., Loros, J. J., and Dunlap, J. C. (2001) The PAS protein VIVID defines a clock-associated feedback loop that represses light input, modulates gating, and regulates clock resetting, *Cell 104*, 453−464.
9. Losi, A., Polverini, E., Quest, B., and Gartner, W. (2002) First evidence for phototropin-related blue-light receptors in prokaryotes, *Biophys. J. 82*, 2627−2634.
10. Crosson, S., and Moffat, K. (2002) Photoexcited structure of a plant photoreceptor domain reveals a light-driven molecular switch, *Plant Cell 14*, 1067−1075.
11. Fedorov, R., Schlichting, I., Hartmann, E., Domratcheva, T., Fuhrmann, M., and Hegemann, P. (2003) Crystal structures and molecular mechanism of a light-induced signaling switch: The Phot-LOV1 domain from *Chlamydomonas reinhardtii*, *Biophys. J. 84*, 2474−2482.
12. Iwata, T., Nozaki, D., Tokutomi, S., Kagawa, T., Wada, M., and Kandori, H. (2003) Light-induced structural changes in the LOV2 domain of *Adiantum* phytochrome 3 studied by low-temperature FTIR and UV−visible spectroscopy, *Biochemistry 42*, 8183−8191.
13. Salomon, M., Eisenreich, W., Durr, H., Schleicher, E., Knieb, E., Massey, V., Rudiger, W., Muller, F., Bacher, A., and Richter, G. (2001) An optomechanical transducer in the blue light receptor phototropin from Avena sativa, *Proc. Natl. Acad. Sci. U.S.A. 98*, 12357−12361.
14. Crosson, S., Rajagopal, S., and Moffat, K. (2003) The LOV domain family: photoresponsive signaling modules coupled to diverse output domains, *Biochemistry 42*, 2−10.
15. Christie, J. M., Swartz, T. E., Bogomolni, R. A., and Briggs, W. R. (2002) Phototropin LOV domains exhibit distinct roles in regulating photoreceptor function, *Plant J. 32*, 205−219.
16. Harper, S. M., Neil, L. C., and Gardner, K. H. (2003) Structural basis of a phototropin light switch, *Science 301*, 1541−1544.
17. Harper, S. M., Christie, J. M., and Gardner, K. H. (2004) Disruption of the LOV-Jalpha helix interaction activates phototropin kinase activity, *Biochemistry 43*, 16184−16192.
18. Lin, C., and Shalitin, D. (2003) Cryptochrome structure and signal transduction, *Annu. Rev. Plant Biol. 54*, 469−496.
19. Brudler, R., Hitomi, K., Daiyasu, H., Toh, H., Kucho, K., Ishiura, M., Kanehisa, M., Roberts, V. A., Todo, T., Tainer, J. A., and Getzoff, E. D. (2003) Identification of a new cryptochrome class. Structure, function, and evolution, *Mol. Cell 11*, 59−67.
20. Galland, P., and Tolle, N. (2003) Light-induced fluorescence changes in *Phycomyces*: evidence for blue light-receptor associated flavo-semiquinones, *Planta 217*, 971−982.
21. Giovani, B., Byrdin, M., Ahmad, M., and Brettel, K. (2003) Light-induced electron transfer in a cryptochrome blue-light photoreceptor, *Nat. Struct. Biol. 10*, 489−490.
22. Gomelsky, M., and Klug, G. (2002) BLUF: a novel FAD-binding domain involved in sensory transduction in microorganisms, *Trends Biochem. Sci. 27*, 497−500.
23. Iseki, M., Matsunaga, S., Murakami, A., Ohno, K., Shiga, K., Yoshida, K., Sugai, M., Takahashi, T., Hori, T., and Watanabe, M. (2002) A blue-light-activated adenylyl cyclase mediates photoavoidance in *Euglena gracilis*, *Nature 415*, 1047−1051.
24. Masuda, S., and Bauer, C. E. (2002) AppA is a blue light photoreceptor that antirepresses photosynthesis gene expression in *Rhodobacter sphaeroides*, *Cell 110*, 613−623.
25. Masuda, S., and Ono, T. A. (2004) Biochemical characterization of the major adenylyl cyclase, Cya1, in the cyanobacterium *Synechocystis* sp. PCC 6803, *FEBS Lett. 577*, 255−258.
26. Kraft, B. J., Masuda, S., Kikuchi, J., Dragnea, V., Tollin, G., Zaleski, J. M., and Bauer, C. E. (2003) Spectroscopic and mutational analysis of the blue-light photoreceptor AppA: a novel photocycle involving flavin stacking with an aromatic amino acid, *Biochemistry 42*, 6726−6734.

27. Laan, W., van der Horst, M. A., van Stokkum, I. H., and Hellingwerf, K. J. (2003) Initial characterization of the primary photochemistry of AppA, a blue-light-using flavin adenine dinucleotide-domain containing transcriptional antirepressor protein from *Rhodobacter sphaeroides*: a key role for reversible intramolecular proton transfer from the flavin adenine dinucleotide chromophore to a conserved tyrosine?, *Photochem. Photobiol. 78*, 290−297.
28. Masuda, S., Hasegawa, K., Ishii, A., and Ono, T. A. (2004) Light-induced structural changes in a putative blue-light receptor with a novel FAD binding fold sensor of blue-light using FAD (BLUF); Slr1694 of synechocystis sp. PCC6803, *Biochemistry 43*, 5304−5313.
29. Rajagopal, S., Key, J. M., Purcell, E. B., Boerema, D. J., and Moffat, K. (2004) Purification and initial characterization of a putative blue light-regulated phosphodiesterase from *Escherichia coli*, *Photochem. Photobiol. 80*, 542−547.
30. Fukushima, Y., Okajima, K., Shibata, Y., Ikeuchi, M., and Itoh, S. (2005) Primary intermediate in the photocycle of a blue-light sensory BLUF FAD-protein, Tll0078, of *Thermosynechococcus elongatus* BP-1, *Biochemistry 44*, 5149−5158.
31. Braatsch, S., Gomelsky, M., Kuphal S., and Klug, G. (2002) A single flavoprotein, AppA, integrates both redox and light signals in *Rhodobacter sphaeroides*, *Mol. Microbiol. 45*, 827−836.
32. Gauden, M., Yeremenko, S., Laan, W., van Stokkum, I. H., Ihalainen, J. A., van Grondelle, R., Hellingwerf, K. J., and Kennis, J. T. (2005) Photocycle of the flavin-binding photoreceptor AppA, a bacterial transcriptional antirepressor of photosynthesis genes, *Biochemistry 44*, 3653−3662.
33. Masuda, S., Hasegawa, K., and Ono, T. A. (2005) Light-induced structural changes of apoprotein and chromophore in the sensor of blue light using FAD (BLUF) domain of AppA for a signaling state, *Biochemistry 44*, 1215−1224.
34. Anderson, S., Dragnea, V., Masuda, S., Ybe, J., Moffat, K., and Bauer, C. (2005) Structure of a novel photoreceptor, the BLUF domain of AppA from *Rhodobacter sphaeroides*, *Biochemistry 44*, 7998−8005.
35. Kita, A., Okajima, K., Morimoto, Y., Ikeuchi, M., and Miki, K. (2005) Structure of a cyanobacterial BLUF protein, Tll0078, containing a novel FAD-binding blue light sensor domain, *J. Mol. Biol. 349*, 1−9.
36. Laan, W., Bednarz, T., Heberle, J., and Hellingwerf, K. J. (2004) Chromophore composition of a heterologously expressed BLUF-domain, *Photochem. Photobiol. Sci. 3*, 1011−1016.
37. Kraayenhof, R., Schuurmans, J. J., Valkier, L. J., Veen, J. P., Van Marum, D., and Jasper, C. G. (1982) A thermoelectrically regulated multipurpose cuvette for simultaneous time-dependent measurements, *Anal. Biochem. 127*, 93−99.
38. Gobets, B., van Stokkum, I. H. M., Rogner, M., Kruip, J., Schlodder, E., Karapetyan, N. V., Dekker, J. P., and van Grondelle, R. (2001) Time-resolved fluorescence emission measurements of photosystem I particles of various cyanobacteria: A unified compartmental model, *Biophys. J. 81*, 407−424.
39. Gradinaru, C. C., Kennis, J. T. M., Papagiannakis, E., van Stokkum, I. H. M., Cogdell, R. J., Fleming, G. R., Niederman, R. A., and van Grondelle, R. (2001) An unusual pathway of excitation energy deactivation in carotenoids: Singlet-to-triplet conversion on an ultrafast time scale in a photosynthetic antenna, *Proc. Natl. Acad. Sci. U.S.A. 98*, 2364−2369.
40. van Stokkum, I. H. M., Larsen, D. S., and van Grondelle, R. (2004) Global and target analysis of time-resolved spectra, *Biochim. Biophys. Acta 1657*, 82−104.
41. Kennis, J. T. M., Crosson, S., Gauden, M., van Stokkum, I. H. M., Moffat, K., and van Grondelle, R. (2003) Primary reactions of the LOV2 domain of phototropin, a plant blue-light photoreceptor, *Biochemistry 42*, 3385−3392.
42. Stanley, R. J., and MacFarlane, A. W. (2000) IV ultrafast excited-state dynamics of oxidized flavins: Direct observations of quenching by purines, *J. Phys. Chem. A 104*, 6899−6906.
43. Nakasako, M., Matsuoka, D., Zikihara, K., and Tokutomi, S. (2005) Quaternary structure of LOV-domain containing polypeptide of *Arabidopsis* FKF1 protein, *FEBS Lett. 579*, 1067−1071.
44. Hoff, W. D., Xie, A., Van Stokkum, I. H., Tang, X. J., Gural, J., Kroon, A. R., and Hellingwerf, K. J. (1999) Global conformational changes upon receptor stimulation in photoactive yellow protein, *Biochemistry 38*, 1009−1017.
45. van der Horst, M. A., van Stokkum, I. H., Crielaard, W., and Hellingwerf, K. J. (2001) The role of the N-terminal domain of photoactive yellow protein in the transient partial unfolding during signalling state formation, *FEBS Lett. 497*, 26−30.
46. Mataga, N., Chosrowjan, H., Taniguchi, S., Tanaka, F., Kido, N., and Kitamura, M. (2002) Femtosecond fluorescence dynamics of flavoproteins: Comparative studies on flavodoxin, its site-directed mutants, and riboflavin binding protein regarding ultrafast electron transfer in protein nanospaces, *J. Phys. Chem. B 106*, 8917−8920.
47. Zhong, D., and Zewail, A. H. (2001) Femtosecond dynamics of flavoproteins: charge separation and recombination in riboflavine (vitamin B2)-binding protein and in glucose oxidase enzyme, *Proc. Natl. Acad. Sci. U.S.A. 98*, 11867−11872.
48. Byrdin, M., Eker, A. P., Vos, M. H., and Brettel, K. (2003) Dissection of the triple tryptophan electron-transfer chain in *Escherichia coli* DNA photolyase: Trp382 is the primary donor in photoactivation, *Proc. Natl. Acad. Sci. U.S.A. 100*, 8676−8681.
49. Gomelsky, M., and Kaplan, S. (1998) AppA, a redox regulator of photosystem formation in *Rhodobacter sphaeroides* 2.4.1, is a flavoprotein, *J. Biol. Chem. 273*, 35319−35325.
50. Han, Y., Braatsch, S., Osterloh, L., and Klug, G. (2004) A eukaryotic BLUF domain mediates light-dependent gene expression in the purple bacterium *Rhodobacter sphaeroides* 2.4.1, *Proc. Natl. Acad. Sci. U.S.A. 101*, 12306−12311.

BI051367P